Atomic-scale three-dimensional kinetic Monte Carlo simulation of organometallic vapor-phase epitaxy of ordered films

C. S. Deo
Princeton Materials Institute, Princeton University, Princeton, New Jersey 08544;
and Department of Mechanical and Aerospace Engineering, Princeton University, Princeton, New Jersey 08544;
and Department of Materials Science and Engineering, University of Michigan, Ann Arbor, Michigan 48109

D. J. Srolovitz
Princeton Materials Institute, Princeton University, Princeton, New Jersey 08544;
and Department of Mechanical and Aerospace Engineering, Princeton University, Princeton, New Jersey 08544
(Received 28 September 2000; published 3 April 2001)

We present an atomistic three-dimensional method for simulating growth of ordered films during organometallic vapor-phase epitaxy (OMVPE). Epitaxial film evolution during growth is studied under typical OMVPE reactor conditions by using a kinetic Monte Carlo technique that incorporates important surface chemical reactions occurring in the reactor. The reactor model consists of a temperature-dependent deposition reaction and a surface etching reaction that depends on the local atomic environment. As a representative ordered film, we study the evolution of an *AB* film on a CsCl lattice. The growth of the epitaxial film is simulated on homoepitaxial, elemental, and disordered substrates with {011} and {001} orientations. Under typical OMVPE conditions, single-crystal homoepitaxial films are observed on homoepitaxial substrates. On elemental and disordered substrate, the film morphology showed domains of opposite orientations separated by antiphase boundaries. In all cases, the growth rate shows an Arrhenius dependence on temperature. Film quality as characterized by the short-range order decreases with increasing temperature. Surface roughness of the epitaxial films corresponds to a staggered surface consisting of a few (2–3) monolayers.

DOI: 10.1103/PhysRevB.63.165411 PACS number(s): 81.15.Aa, 05.10.Ln, 68.03.Fg, 81.15.Kk

INTRODUCTION

Organometallic vapor-phase epitaxy (OMVPE) is extensively used to produce high-quality epitaxial films of compound semiconductors, ferroelectrics, superconductors, and magnetic materials for a wide range of technological applications.[1] The properties (resistivity, band-gap energy, dielectric permittivity, superconductivity, etc.) of OVMPE films can vary dramatically with reactor conditions. Thus, our ability to tailor film properties for particular applications depends on our ability to predict the relationships between reactor conditions, film structure, and film properties. This will serve both as guidance for designing film growth protocols and the control strategies for high-quality epitaxial film growth. One difficulty in developing this predictive understanding of OMVPE is our inability to directly observe the evolving film structure during growth with atomic resolution. At the same time, theoretical analyses of the OMVPE process is hindered by the complexity of the chemical reactions (i.e., large number of species, complex precursor molecules, uncertain kinetic pathways, etc.) in the gas phase, in the boundary layer, and on the surface of the growing film. Molecular simulations provide one mechanism for accessing the evolving structure during film growth and provide a means for sorting out atomistic growth mechanisms, predicting growth rates, and establishing the difficult link between reactor conditions and film structure.

Two main approaches are available for simulating the film growth at the molecular level: namely, molecular dynamics (MD) and kinetic Monte Carlo (kMC) methods. Molecular-dynamics methods are extremely powerful and can be used to predict all of the chemical reactions and dynamics occurring on the growth surface provided that a sufficiently robust description of the atomic interactions is available (typically this is only possible using quantum mechanically based descriptions). Standard molecular dynamics implementations are capable of following the evolution of the structure over times ranging from fs to ns. While new methods are being developed to increase this time scale (e.g., Ref. 2), this limitation is severe given growth rates that typically do not exceed 1 nm/sec in OMVPE of compounds. Kinetic Monte Carlo methods can be used to study growth phenomena on both larger length and considerably longer time scales. On the other hand, kMC methods replace the true atomic scale dynamics with statistically equivalent kinetics, provided that the relative rates of all important dynamical phenomena are available. In principle, such rates can be determined from quantum-mechanical calculations, MD simulations, and experiment. Kinetic Monte Carlo methods have been successfully applied to the growth of single component films such as diamond via chemical vapor deposition (CVD) (Refs. 3–5) and silicon via pulsed laser deposition and molecular beam epitaxy (MBE).[6]

Most epitaxial films of commercial interest produced by OMVPE are multicomponent compound semiconductors[7] ($Al_xGa_{1-x}As$, $Ga_xIn_{1-x}As$, $Ga_xIn_{1-x}P$, etc.), superconductors[8] ($YBa_2Cu_3O_{7-x}$, $La_{2-x}Sr_xO_4$), or ferroelectric oxides[9] ($BaTiO_3$, $SrTiO_3$, $PbZrO_3$, etc.). As the name implies, at least one of the depositing species in OMVPE is introduced into the reactor in the form of an organometallic precursor. Reactions in the vapor phase or on the surface lead to the

deposition of metallic or molecular species. The surface species may diffuse along the surface, desorb back to the vapor, or further react to produce an elemental cation or anion or the compound itself. Thus reactions between the vapor and surface or on the surface and surface transport can all play important roles in determining the structure and characteristics of the epitaxial film. Different growth regimes are possible, depending on the thermodynamic and kinetic parameters that dictate reaction rates, reaction mechanisms, and transport phenomena. Kinetic Monte Carlo methods provide ideal vehicles to examine the interplay between these thermodynamic and kinetic phenomena.

Several kMC simulations have been performed to investigate the growth of two component films. Blue *et al.*[10] simulated the MBE growth of Co/Cu (100) alloy films.[11] Gallivan *et al.*[12] examined the OMVPE deposition of YBCO in the spiral growth mode under nonsteady state conditions in which they described the entire YBCO unit cell as the growth species. Kinetic Monte Carlo simulations have also been used to study growth induced domain coarsening and surface roughening phenomena of a generic $A_{0.5}B_{0.5}$ film during molecular beam epitaxy.[13] All of these simulations were based on a solid-on-solid (SOS) (Ref. 14) description of the film structure. The SOS model is a $(2+1)$-dimensional model in which the surface of the film is a single valued value function of the coordinates in the plane of the substrate $h(x,y)$. This reduced dimensional construction does not allow for incorporated vacancies in the film or complex surface morphologies. These implementations of the SOS model focused on the growth surface and did not track the film structure below the surface. In multicomponent films, the key structural characteristics of the film are the degree of ordering and the incorporation of defects (vacancies, stacking faults, antisite defects). Solid-on-solid model descriptions are also incapable of describing the type of multiatomic-plane ordering that is fundamental to the growth of compound films (e.g., *c*-oriented YBCO has a six metal plane repeat sequence: Cu-Ba-Cu-Y-Cu-Ba, where we have omitted the oxygen atoms). A truly three-dimensional model is necessary to describe all of these important issues in the growth of multicomponent films by OMVPE.

In this paper, we present a three-dimensional, atomistic simulation method for the growth of ordered films under typical OMVPE conditions, building on our earlier work on diamond CVD.[3] The goal of this paper is the development of a simulation model capable of describing the full physical complexity of the growth of compound films. The simulations are based on a relatively simple set of reactions representing the deposition and etching of two species *A* and *B*. The reaction kinetics are sensitive to the local environment and the thermodynamic parameters are chosen to favor compound formation. We examine the evolution of the film structure as a function of substrate temperature, reactor pressure, partial pressures of precursors, and substrate type. The resultant microstructures are analyzed to determine domain structure, short-range order, and surface roughness.

MODEL

As a representative multicomponent system, we considered an ordered *AB* alloy with the *B*2 (CsCl) crystal structure, which can be viewed as two interpenetrating simple cubic sublattices (arbitrarily labeled as α and β, below) which, in a perfect CsCl crystal, are occupied exclusively by two different types of atoms. If atom types *A* and *B* are identical, then this lattice becomes body centered cubic. The simulation cell consists of a three-dimensional lattice of atomic sites in space. Periodic boundary conditions are imposed in the plane of the film (i.e., in the *x* and *y* directions). At the beginning of each simulation, the substrate is constructed by occupying the lowest atomic planes by the substrate atoms up to a thickness of one unit cell. Several types of substrates are considered: (i) the same as the *AB B*2 film, (ii) single atomic type (pure *A* or *B* in a body centered cubic structure), and (iii) a random *AB* solid solution alloy (equal *A* and *B* concentration and body centered cubic). The first case corresponds to homoepitaxial growth, while the latter two to zero misfit, heteroepitaxial growth. The initial substrate interacts with a gas phase containing the organometallic precursors, leading to the deposition of atomic species.

In order to represent the deposition of the atomic species, we employ a simple kinetic model that incorporates irreversible temperature-dependent adsorption reactions and reversible etching reactions:

$$AX_1(g) \rightarrow A(s) + \text{gas-products}, \tag{1}$$

$$AX_2(g) \leftrightarrow A(s) + X_2(g), \tag{2}$$

$$BY_1(g) \rightarrow B(s) + \text{gas-products}, \tag{3}$$

$$BY_2(g) \leftrightarrow B(s) + Y_2. \tag{4}$$

In this simple model, AX_1 and BY_1 are the organometallic precursor in the chemical reactor and X_2 and Y_2 are the by-products of their dissociation. In the deposition of $BaTiO_3$, for example, *A*, *B*, AX_1, and BY_1 may be barium oxide, titanium oxide, barium tetraglyme, and titanium isopropoxide, respectively. Reactions (1) and (3) are dissociation reactions for the precursors AX_1 and BY_1. The reverse of reactions (2) and (4) represent the etching of deposited species from the surface. The kinetic parameters and the typical partial pressures of gases in the reactor employed in the simulation are given in Table I. As a matter of convenience, we use reduced units for energy (ε), volume (V), temperature (ε/k_B), pressure (ε/V), and time (τ).

Using this data, the forward and reverse reaction rate constants (k_f and k_r) are computed as follows:

$$k_f = AT^n \exp\left(-\frac{E}{T}\right), \tag{5a}$$

$$k_r = AT^n \exp(-\Delta S)\exp\left(\frac{\Delta H - E}{T}\right), \tag{5b}$$

where E is the kinetic barrier for the reaction, T is the temperature, and k_B is the Boltzmann constant. ΔH and ΔS are the enthalpy and entropy change of the reaction at equilibrium. ΔH is taken as the binding energy ΔH_b for the atomic species, which is calculated as follows:

TABLE I. Reaction rate parameters for the growth of the ordered AB films. A' is in units of ς/τ, E and ΔH and are in units of ε, ΔS is in units of k_B, P_i in units of ε/ς, partial pressures of the precursors are variables.

	Reaction	A'	E	ΔH	ΔS	P_i
(1)	$AX_1(g) \rightarrow A(s) + \text{products}$	1.0×10^{15}	15.0	ΔH_b	0.0	P_{AX_1}
(2)	$AX_2(g) \leftrightarrow A(s) + X_2(g)$	2×10^{15}	1.0	ΔH_b	0.0	P_{AX_2}, P_{X_2}
(3)	$BY_1(g) \rightarrow B(s) + \text{products}$	1.0×10^{15}	15.0	ΔH_b	0.0	P_{BY_1}
(4)	$BY(g) \leftrightarrow B(s) + Y_2(g)$	2.0×10^{15}	15.0	ΔH_b	0.0	P_{BY_2}, P_{Y_2}

$$\Delta H_b = n_{AA}\varepsilon_{AA} + n_{AB}\varepsilon_{AB} \quad \text{for atomic species } A, \tag{6a}$$

$$\Delta H_b = n_{BB}\varepsilon_{BB} + n_{AB}\varepsilon_{AB} \quad \text{for atomic species } B. \tag{6b}$$

Here, n_{ij} is the total number of bonds going from species i to nearest neighbors of species j (note $n_{AB}=n_{BA}$). Thus, the enthalpy and, hence, the rate of the etching reaction depends on the local environment of the deposited species.

In order to get a feel for the values of the parameters employed (Table I), we can set $\varepsilon=1$ kcal/mole, such that a temperature of $1\varepsilon/k_B$ corresponds to 503.48 K. In the present simulations, we set $\varepsilon_{AA}=\varepsilon_{BB}=-\varepsilon$ and -5ε ε_{AB} -10ε. With this value of ε, the cohesive energy of pure A or pure B (bcc) is 8 kcal/mole and that of the $B2$ AB alloy is between 40 and 80 kcal/mole (i.e., ordering is strongly thermodynamically favored). The unit of volume V is a^3, where a is the lattice parameter ($a=0.283$ nm) and the unit of time $\tau=1$ sec. The other parameters are scaled appropriately.

For reactions involving gas phase reactants, the reaction rate is obtained by multiplying the reaction rate constants by the ideal partial molar volume of the gas phase reactants

$$r = \frac{P_i}{RT}k, \tag{7}$$

where P_i is the partial pressure of gas phase component i. P_i and T are inputs to the model. The partial pressures of the gas phase component i may be thus expressed as $P_i=c_iP$, where c_i is the mole fraction of reactant i gas in the chamber and P is the total reactor pressure.

The rates of the reactions occurring at each surface site are taken as input for the kinetic Monte Carlo (kMC) algorithm. The probability that a particular reaction will occur next is proportional to the rate of that reaction. Given the rates of all the reactions at all surface sites, the kMC algorithm selects both a surface site and reaction and adjusts the simulation clock according to the total rate that any reaction will occur. More formally, we write the probability of occurrence for each event (site and reaction) as the ratio of its reaction rate to the sum of all the reaction rates in the simulation. At each simulation step, event m is selected according to

$$\frac{\sum_{i=1}^{m-1} r_i}{\sum_{i=1}^{M} r_i} < \zeta_1 < \frac{\sum_{i=1}^{m} r_i}{\sum_{i=1}^{M} r_i}, \tag{8}$$

where ζ_1 is a random number chosen between [0,1), M is the total number of events that could occur anywhere in the simulation cell at that instant, and r_i is the reaction rate of event i. The occupancies of the selected sites (A, B, or empty) is changed in accordance with the selected reaction and the event list is updated for this site and its neighbors. This procedure is then repeated in the next Monte Carlo (MC) step. At each simulation step, the time increment is variable and stochastic, and is calculated as follows:

$$dt = \frac{-\ln(\zeta_2)}{\sum_{i=1}^{M} r_i}, \tag{9}$$

where ζ_2 is a random number between (0,1] and dt is the time increment. The use of a variable time increment allows the algorithm to be flexible in consideration of reactions that occur on widely disparate time scales.[15] When the event list contains fast reactions (large reaction rates), the denominator in Eq. (9) is large and the time increment is small. When only slow reactions are possible, the denominator in Eq. (9) is small, and the simulation clock is incremented by a large value. This algorithm is similar to the N-fold way method,[16,17] which has been shown to yield statistically equivalent results to the more traditional (Metropolis[18]) fixed time step algorithm. The present algorithm is more flexible while handling events that occur with widely disparate rates, as in cases involving diverse chemical reactions—such as in OMVPE.

A schematic illustration of the initial few steps in the evolution of a very small fragment of the film is shown in Fig. 1. The growth is occurring on a flat homoepitaxial {011} oriented surface, where light circles indicate A atoms and dark circles represent B atoms. Initially, the equiatomic {011} plane [Fig. 1(a)] has N surface sites ($N=32$ here). Four deposition reactions [the forward reactions from Eqs. (1)–(4)] are possible at each site, and each surface atom can be etched [the reverse reactions from Eqs. (2) and (4)], thus $5N$ events are possible at the first kMC step (deposited atoms are indicated by a + sign in the figure). The kMC algorithm selects an event, according to Eq. (8), and the occupancies of the sites change according to this choice. Figures 1(b) and 1(c) show two of the possible events that can occur. If the event that leads to the deposition of the A atom [as shown in Fig. 1(b)] is chosen, there are $4(N+1)$ adsorption reactions [forward reactions in Eqs. (1)–(4)] and N etching reactions [reverse of Eqs. (2) and (4)] possible (in the event list) for the next kMC step. In general, if an adsorbed A atom on an

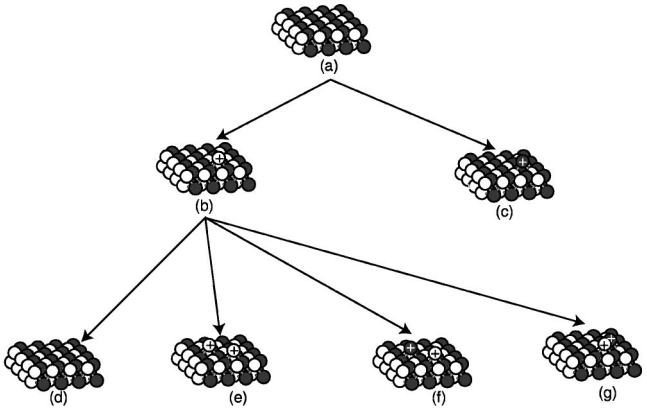

FIG. 1. Evolution of a fragment of ordered *AB* film on a homoepitaxial substrate of {011} orientation. Light circles indicate *A* atoms and dark circles indicate *B* atoms. The atoms marked with + are deposited atoms. Initially, the flat substrate (a) can undergo adsorption of an *A* atom (b) or adsorption of *B* atom (c). Evolution from (b) occurs by etching of the adsorbed *A* atom (d), adsorption of another *A* atom (e), or adsorption of a *B* atom (f),(g). In plane bonding on the surface with {011} orientation leads to the formation of nuclei of *A*-*B* atom pairs (g) on the surface.

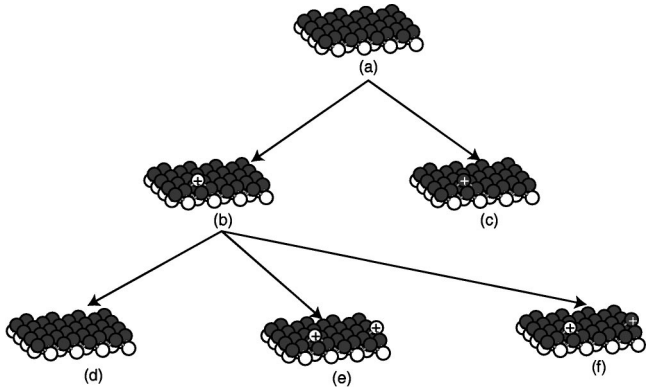

FIG. 2. Evolution of a fragment of ordered *AB* film on a homoepitaxial substrate of {001} orientation. Initially, the flat substrate (a) can undergo adsorption of an *A* atom (b) or adsorption of *B* atom (c). Evolution from (b) occurs by etching of the adsorbed *A* atom (d), adsorption of another *A* atom (e), or adsorption of a *B* atom (f). There is no in plane bonding on surfaces with {001} orientation.

otherwise flat surface has 2 *B* neighbors, the binding energy ΔH_b has a very large negative value, thus the rate for etching is very low, and the etching event has low probability of being selected by the kMC algorithm in the next kMC step. If the deposited *A* atom has 2 *A* neighbors the binding is weak, and the etching rate is very high and will likely be selected in the next kMC step. If such an etching reaction is selected, the system reverts to the initially flat surface [Fig. 1(d)]. If an adsorption reaction on another site is selected rather than an etching reaction, the system progresses to one of the configurations shown in Figs. 1(e)–1(g). Whichever event occurs next, the occupancies of the sites are changed to reflect the execution of this step, and the event list is recalculated to serve as input to the next kMC step.

The evolution of a film fragment with a {001} oriented surface is shown in Fig. 2. The film evolves in a manner similar to the evolution of the {001} oriented film in Fig. 1. The flat {001} surface has alternately pure *A* and pure *B* layers (unlike the {001} oriented surface in Fig. 1). For the fragment of film shown in Fig. 2(a), $5N$ reaction events are possible. In general, an atom on a flat terrace is bonded to four neighbors in the surface below. Thus an *A* atom on a flat terrace [Fig. 2(b)] is strongly bound if its local environment contains 4 *B* atoms. Etching of such an atom [Fig. 2(d)] will occur at a much lower reaction rate compared to the deposition of another atom [Figs. 2(e) and 2(f)]. Thus deposition of another atom *A* will occur much more likely on this *B* surface during the next kMC step. Figures 1 and 2 demonstrate that although the local bonding is different on the two surfaces, the deposition rates are equal. On the other hand, the etching rate of a deposited atom is very sensitive to the local bonding environment [see Eqs. (5) and (6)].

The preceding examples considered the evolution of the film structure by the chemisorption or etching of atoms from solid surface sites. An atom is completely incorporated into the film once all of its neighboring sites are occupied by either *A* or *B* atoms. It is possible that an empty site (or vacancy) will be incorporated into the growing film if all of the neighbors of this site become occupied such that this site no longer has access to the gaseous environment. This vacant site will remain in the film unless one or more of its filled neighbor sites is etched away.

The present model does not include diffusional events on the growing film surface. While such events are clearly important during the OVMPE in many systems they are omitted from the present model in order to simplify interpretation of the results and to focus on the chemical reaction steps that are occurring on the surface during growth. The present model is easily extended to include surface diffusion. However, doing so would necessitate the introduction of a large number of additional parameters in the present model. These parameters are generally unknown both in the quantitative sense and relative to the other physical parameters in the simulation.

FILM STRUCTURE

Growth on {011} oriented homoepitaxial substrates

Figure 3 shows the evolution of the surface morphology during the homoepitaxial growth of a {011} oriented film at a low temperature ($T=1\varepsilon/k_\beta$). This film was grown with $\varepsilon_{AB}=-5\varepsilon$ in a reactor at a total pressure of $10^{-6}\,\varepsilon/V$, with a gas phase environment of $C_i=0.5$, 0.5, 0.05, or 0.05 mole fraction where $i=AX_1$, BY_1, X_2, or Y_2, respectively, and with negligible traces of gaseous AX_2 and BY_2. Each atomic layer consists of 2048 atomic sites and the (homoepitaxial) substrate was two layers thick. Several distinct single atomic height islands are first nucleated (see below) on the substrate. These islands grow in-plane by the addition of atoms to the step edges. Before the first layer is complete, additional islands nucleate on the surface of this layer, starting the second layer. As the deposition proceeds, growth continues on 2–3 layers simultaneously. The resultant structure consists of

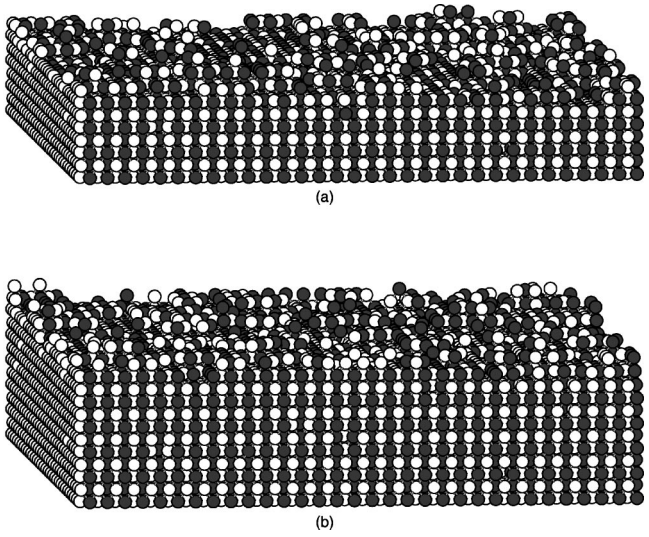

FIG. 3. Growth of a film on a large homoepitaxial substrate with {011} orientation at temperature of $1\varepsilon/k_B$, with $\varepsilon_{AB}=-5\varepsilon$, reactor pressure of 10^{-6} ε/V, and a gas phase environment $C_i=0.5$, 0.5, 0.05, or 0.05 mole fraction where $i=AX_1$, BY_1, X_2, or Y_2, respectively, and with negligible traces of gaseous AX_2 and BY_2. The *A* atoms are shown in black and the B atoms in white.

well-defined terraces, bound by kinked steps. This growth is nearly layer-by-layer, with a typical terrace size of approximately 15 atomic diameters.

On a flat, ordered {011} substrate or surface, an adsorbed atom has either two like or two unlike neighbors. If an adsorbed *A* atom has two *A* neighbors, the magnitude of the binding energy ΔH_b is small and the rate of etching is high. If the *A* atom has two *B* neighbors, the rate of etching is much smaller. In either case, a single atom on a terrace does not constitute a stable nucleus and is easily etched off the surface. An isolated atom on the surface can be stabilized by the deposition of another atom of the opposite type into one of its nearest neighbor (in-plane) sites. Since the first atom has a very short residence time on the surface, if it is not in a proper homoepitaxial site (i.e., a proper site is one in which the neighbors below are of the opposite type), the rate of formation of two atom nuclei with the proper orientation is much greater than for phase shifted nuclei. This is because the atoms in a properly oriented nucleus have three neighbors of opposite type. This two atom pair is further stabilized by addition of more neighboring atoms of the proper type. An atom adsorbed on the next layer is more likely to be etched than an atom adsorbed onto the edge of a nucleus (step edge). Thus, in plane growth is more favored than out of plane growth on a homoepitaxial {011} substrate under typical growth conditions. This constitutes a step-growth mechanism.

Growth on {001} oriented homoepitaxial substrates

Figure 4 shows the homoepitaxial growth of a {001} oriented film under the same conditions as in Fig. 3 (i.e., as in the {011} substrate described above). In this substrate orientation, the film is composed of alternating layers of pure *A* and pure *B*. The surface of the growing film shows both terraces (the terrace size at late times is 20 atomic diameters) as well as some isolated atoms. As on the {011} oriented film, this surface is relatively flat (to within approximately three monolayers). Atoms on the wrong sublattice are rare, i.e., ordering is preserved during growth.

On homoepitaxial {001} substrates, an adsorbed atom on a flat, ordered terrace has four bonds to atoms in the terrace. These atoms can either be all like or all unlike the adsorbed atom. If an adsorbed *A* atom has four *A* neighbors, the magnitude of the binding energy ΔH_b is small, and the rate of etching is high. If it has four *B* neighbors, the rate of etching is much lower since the binding is strong (i.e., ΔH_b is large and negative). There are no in-plane bonds in an {001} oriented film, such that growth at a step is no more favorable than growth on a terrace. However, an adsorbed atom will only remain on the surface for a long time if all four of its nearest neighbor sites in the terrace are occupied. This prevents the film from getting very rough, but also keeps the terrace size relatively small.

Growth on {011} oriented elemental substrates

Epitaxial growth on an {011} oriented, elemental substrates is shown in Fig. 5 under the same conditions as in Figs. 3 and 4. Both the α and β sublattices of the substrate are occupied by *A* atoms. As the film grows, islands form both with *A* atoms on the α sublattice and with *A* atoms on the β sublattice. The average steady-state terrace size is approximately 10 atomic diameters. When these islands grow together, antiphase boundaries (APB's) form. A plan-view section of the film [Fig. 5(c)] shows that the antiphase boundaries are highly curved and the domain shapes are not compact. Examination of the sides of the model [Fig. 5(b)] show that the domain size increases as the film thickens. This

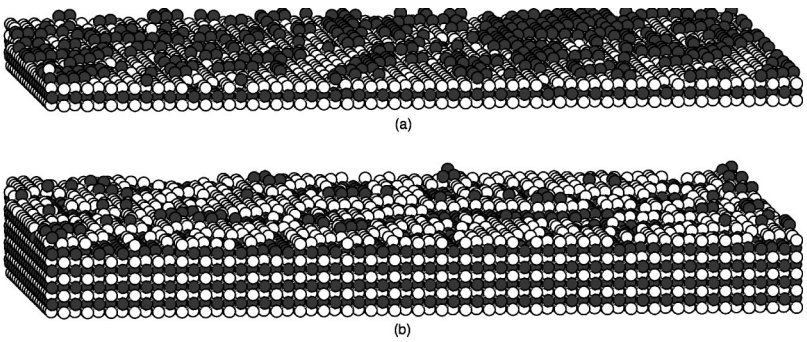

FIG. 4. Evolution of the film on a large homoepitaxial substrate with {001} orientation under the same conditions as in Fig. 3.

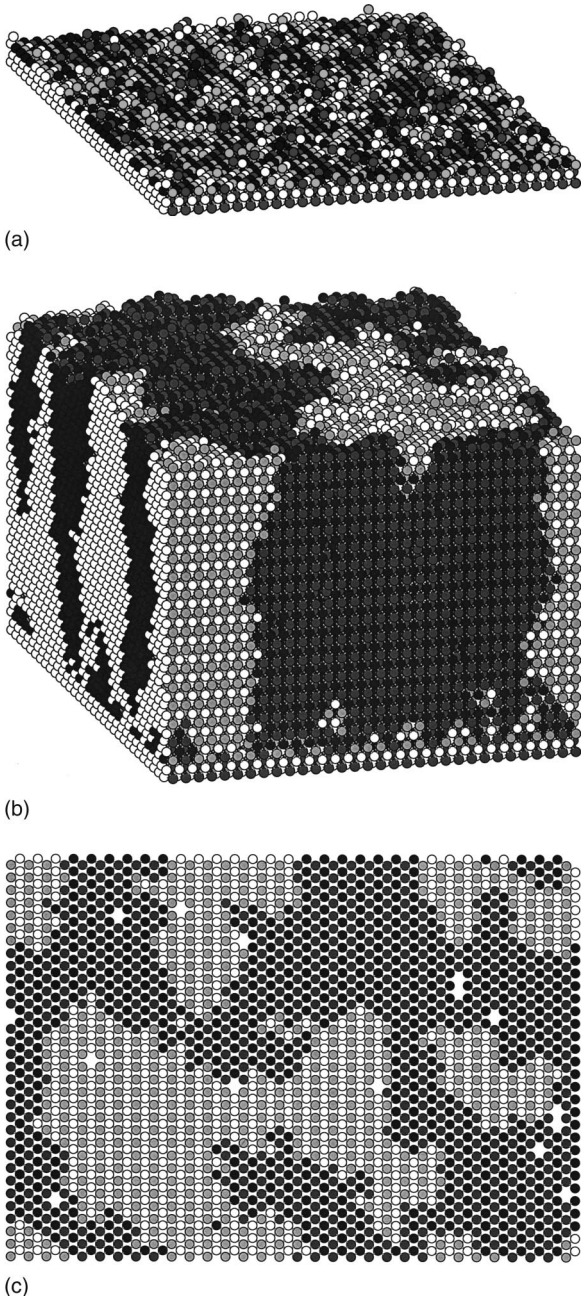

FIG. 5. Evolution of the film on a large, {011} oriented, elemental substrate at temperature of $1\varepsilon/k_B$, with $\varepsilon_{AB}=-5\varepsilon$, under the same reactor conditions as in Fig. 3. (a) and (b) show the film at two different stages of growth and (c) is a slice of the film parallel to the substrate at a film thickness of $8a$. The shading of the atoms was chosen to highlight the two domain orientations: black and light gray atoms are *A* atoms and the white and dark gray atoms are *B* atoms.

evolution is rapid near the substrate and the walls of the APB's become increasingly vertical far from the substrate. This ''domain pinching'' effect results in relatively large domains. Experimental observations of the structure of epitaxially grown films of binary alloys show a similar evolution of the domain structure,[7,19,20] with typical cross sections exhibiting domains that are nearly parabolic. Landau *et al.*[13] reported similar APB's and coarsening during kMC simulations of MBE growth of $A_{0.5}B_{0.5}$ films.

Initially an adsorbed *A* atom on the pure *A* substrate is etched more rapidly than an adsorbed *B* atom, although any isolated atom on the flat substrate is easily etched. As in the case of growth on homoepitaxial substrates, islands of two or more atoms are more stable than a single atom on the substrate or on a terrace. This favors growth by a step mechanism, as discussed above. Since there is no preference for the phase of the individual islands on the substrate, the islands are commonly out-of-phase with respect to each other—giving rise to APB's. The APB structure coarsens as the film thickens because atoms are etched from the surface more slowly the larger number of unlike neighbors they have. Atoms can find more such neighbors on the outer surface of a curved APB than on the inner surface. This is simply the Gibbs-Thompson effect.[21] Therefore, the coarsening of the APB structure is controlled by capillarity (i.e., APB energetics and curvature).

Growth on {011} oriented disordered substrates

Epitaxial growth on an {011} oriented, but disordered substrates is shown in Fig. 6 under the same conditions as in Figs. 3–5. The α and β sublattices of the substrate are randomly occupied by *A* and *B* atoms (with equal probability). In this case, the local neighbor environment of the adsorbed *A* and *B* atoms on the substrate can be homoepitaxial, *A*-rich or *B*-rich. Thus, nuclei of both phase form on the substrate. The resultant islands grow together producing APB's. The average steady-state terrace size is about 10 atomic diameters. The domain size increases with increasing film thickness. The initial domain size in the disordered substrate case (Fig. 6) is smaller than in the elemental substrate case (Fig. 5) at the same film thickness. This is likely associated with the large densities of locally homoepitaxial atomic arrangements (of both phases) on the disordered substrate which provides easy nucleation of both domains, while in the elemental substrate case nucleation of domains of either phase is considerably slower (allowing more time for selective etching from island edges).

GROWTH RATES

The variation of film growth rates with temperature is shown in Fig. 7 for deposition onto a homoepitaxial {011} oriented substrates for several different values of the *A*-*B* bond strength ($\varepsilon_{AB}=-5\varepsilon$, $\varepsilon_{AB}=-6\varepsilon$, $\varepsilon_{AB}=-7\varepsilon$). Additional simulations were performed on homoepitaxial, elemental, and disordered {001} and {011} substrates. The plots for these additional cases are very nearly indistinguishable from that in Fig. 7. In all cases, the simulations were performed at reactor pressure of $10^{-6}\varepsilon/V$, with a gas phase environment of $C_i=0.5$, 0.5, 0.05, or 0.05 mole fraction where $i=AX_1$, BY_1, X_2, or Y_2, respectively, and with negligible traces of gaseous AX_2 and BY_2. The growth rate R shows an Arrhenius dependence on temperature,

$$R=A\exp\left(-\frac{\eta}{k_BT}\right), \tag{10}$$

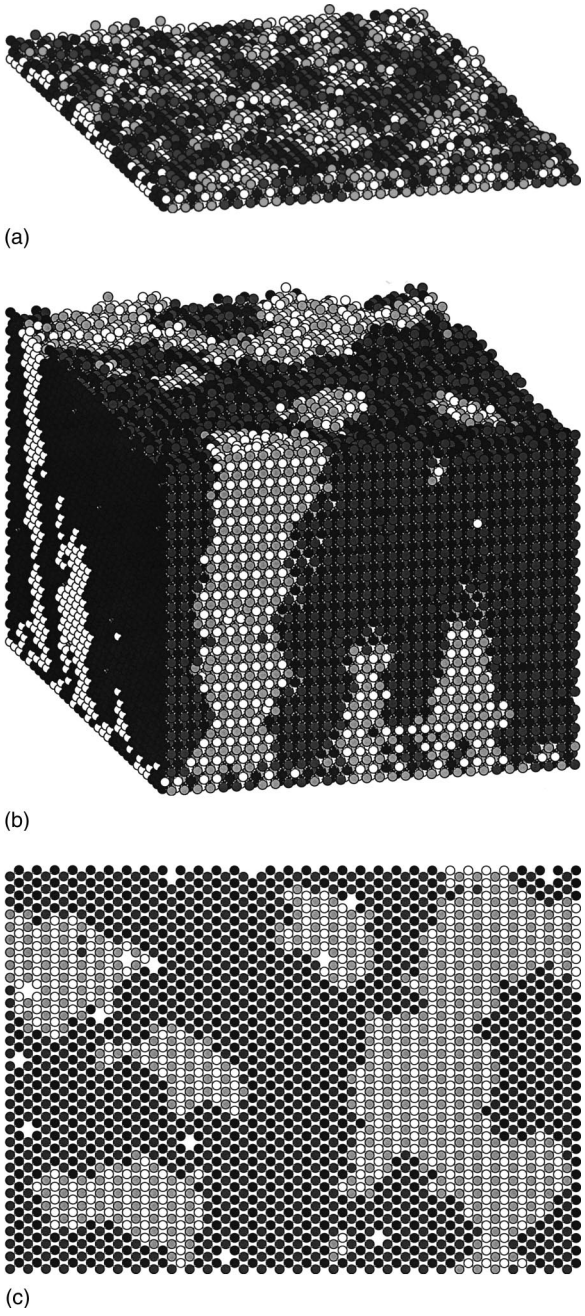

FIG. 6. Growth of the film on a large, {001} oriented, elemental substrate at a temperature of $1\varepsilon/k_B$, with $\varepsilon_{AB}=-5\varepsilon$, under the same reactor conditions as in Fig. 3. (a) and (b) show the evolution of the film at two different stages of growth and (c) is a slice of the film parallel to the substrate at a film thickness of $8a$.

where A and η are constants. The growth rates are very nearly independent of substrate type of substrate orientation. The growth rate increases very slowly with increasing *A-B* bond strength. Similarly, the growth rates increase with increasing partial pressure of the reactants AX_1 and BY_1, as expected based on the explicit pressure dependence of the reaction rates in Eq. (7). For the values of the activation energies chosen above, the growth is reaction rate limited rather than reactant flux limited, as often occurs. Reactant flux controlled growth could be recovered by changing the

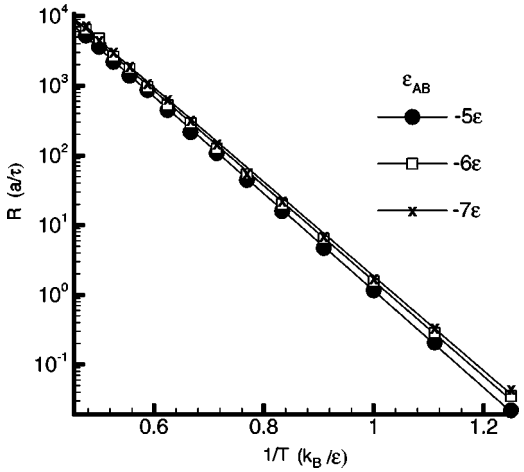

FIG. 7. Growth rate as a function of the inverse temperature for different values of ε_{AB} with a reactor pressure of 10^{-6} ε/V for the same conditions as in Fig. 3. These simulations were performed on a {011} oriented, homoepitaxial substrate.

parameters in Eqs. (1) and (3).

The values of the parameters A and η were extracted from the slopes of the curves in Fig. 7. These data (averaged over all six cases) suggest that the activation energy $\eta=15.6\pm0.4\varepsilon$ and the pre-exponential factor $A=9.94\pm0.37\times10^6 a/\tau$ and are very nearly independent of substrate type and bond strength. This activation energy is very close to the activation energy for the decomposition of the precursors [i.e., Eqs. (1) and (3)], $E=15.0\varepsilon$. This demonstrates that the growth kinetics in this OMVPF model are dominated by the rates at which the precursors decompose on the surface.

SURFACE ROUGHNESS

The surface roughness δ is plotted as a function of film height (h) for different values of the bonding parameter ε_{AB} (Fig. 8) at $T=1\varepsilon/k_B$ and for different values of the temperature (Fig. 9) at fixed $\varepsilon_{AB}(=-5\varepsilon)$ for homoepitaxial growth on {011} and {001} substrates. In all cases, simulations were performed for a reactor pressure of $10^{-6}\varepsilon/V$ and a gas phase environment of $C_i=0.5$, 0.5, 0.05, or 0.05 mole fraction where $i=AX_1$, BY_1, or X_2, or Y_2, respectively, and with negligible traces of gaseous AX_2 and BY_2. Similar plots for growth on the elemental and disordered substrates were nearly indistinguishable. The roughness δ is defined here as the standard deviation of the film height (root mean square deviation)

$$\delta^2=\frac{1}{N}\sum_{i=1}^{N}(h_i-\overline{h})^2, \tag{11}$$

where h_i is the shortest distance between the substrate and surface site i,$\overline{h}$ is surface height averaged over all N surface sites.

The roughness initially shows a rapid increase with film height before asymptotically approaching a steady state. The steady-state roughness lies between $0.5a$ and $0.8a$ for {011} oriented films. The steady-state roughness lies between

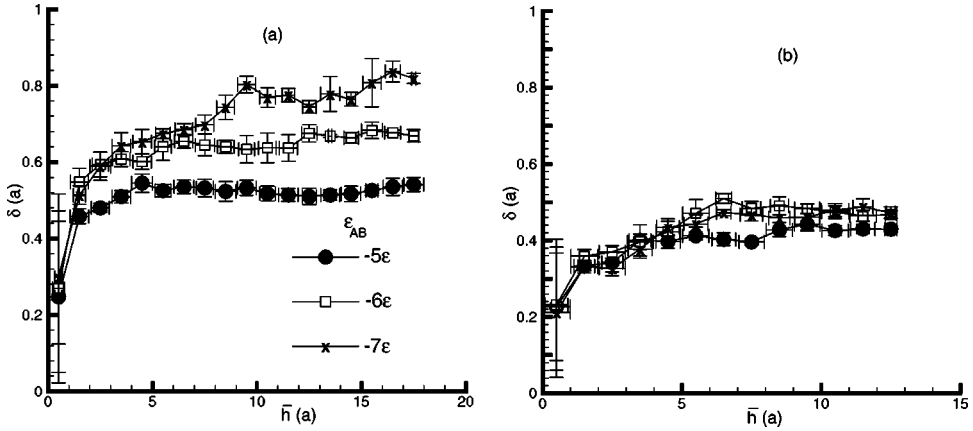

FIG. 8. Surface roughness as a function of the average film height for different values of ε_{AB} at a temperature of $1\varepsilon/k_B$, with the reactor pressure of 10^{-6} ε/V for the same conditions as in Fig. 3. These simulations were performed on (a) {011} oriented, homoepitaxial substrates and (b) {001} oriented, homoepitaxial substrates. Vertical error bars indicate standard deviation about the mean, while horizontal error bars indicate the standard deviation of the data in each bin over four simulations.

$0.35a$ and $0.5a$ for {001} oriented films. For both film orientations, this roughness is close to a single interplanar spacing (i.e., one monolayer). This spacing is $a/\sqrt{2}$ for {011} and $a/2$ for {001}. Figures 8 and 9 show that there is very little change upon changing either the *A-B* bond strength or temperature within the ranges examined here. One exception is the bond strength dependence of the roughness of the {011} oriented films on homoepitaxial substrates. In this case, the steady-state roughness clearly increases with increasing ε_{AB} [Fig. 8(a)].

The initial quick rise in δ with increasing thickness is associated with nucleation and island growth on an initially perfectly flat substrate. The roughness begins to asymptote after approximately one monolayer, where nucleation on a flat surface ceases (the initial terrace sizes are very small).

The variation of the roughness of the {011} oriented film on a homoepitaxial substrate with *A-B* bond strength can be understood in terms of the competition between step growth and nucleation on terraces. As described above, this film tends to grow predominantly by a step growth mechanism. However, increasing the *A-B* bond strength increases the stability of *A-B* nuclei on {011} terraces. Since the growth of new islands on {011} terraces increases film roughness, increasing *A-B* bond strength should lead to rougher surfaces, as seen in the simulation data in Fig. 8(a). This effect is missing in the {001} oriented films [Fig. 8(b)]. This is because the step growth mechanism does not operate during the growth of {001} oriented films. The lack of variation of the asymptotic surface roughness of the {011} films grown on elemental or disordered substrates (not shown) with the *A-B* bond strength must be associated with the presence of antiphase boundaries. The terrace sizes are much smaller when APB's are present than when they are absent (cf. see Figs. 3, 5, and 6). Since the formation of nuclei on ideal {011} terraces becomes geometrically less likely with decreasing terrace size, the contribution to roughening associated with the additional stability of the nuclei on {011} terraces with increasing *A-B* bond strength is much less relevant when APB's are present. This decreased terrace size with increased APB density washes out the *A-B* bond strength effect.

Figure 9 shows that the effect of temperature on film roughness is negligible for films grown on all substrate types and orientations examined. Since changing temperature modifies all of the reaction rates differently (depending on the values of the activation energies and ΔH), this temperature independence of the roughness is surprising—especially in the case of {011} oriented films on homoepitaxial substrates (for the reason described above). However, since the activation energy for deposition and the values of ΔH associated with formation of an *A-B* pair are very similar [see Table I and Eqs. (5) and (6)], changing the temperature does little to the relative stability of *A-B* pairs. Hence, changing temperature does little to bias the competition between nucleation on terraces and step growth, resulting in nearly temperature independent roughness.

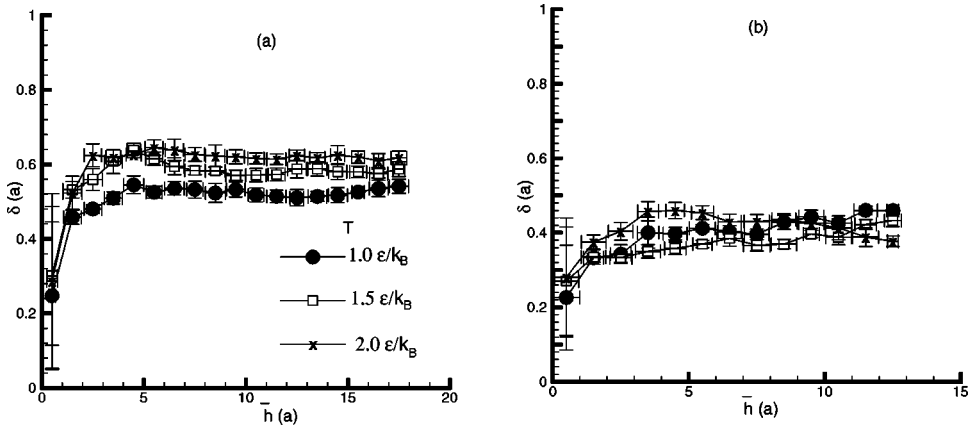

FIG. 9. Surface roughness as a function of the average film height for three different values of temperature with $\varepsilon_{AB}=-5\varepsilon$, reactor pressure of 10^{-6} ε/V for the same conditions as in Fig. 3. These simulations were performed on (a) {011} oriented, homoepitaxial substrates and (b) {001} oriented, homoepitaxial substrates.

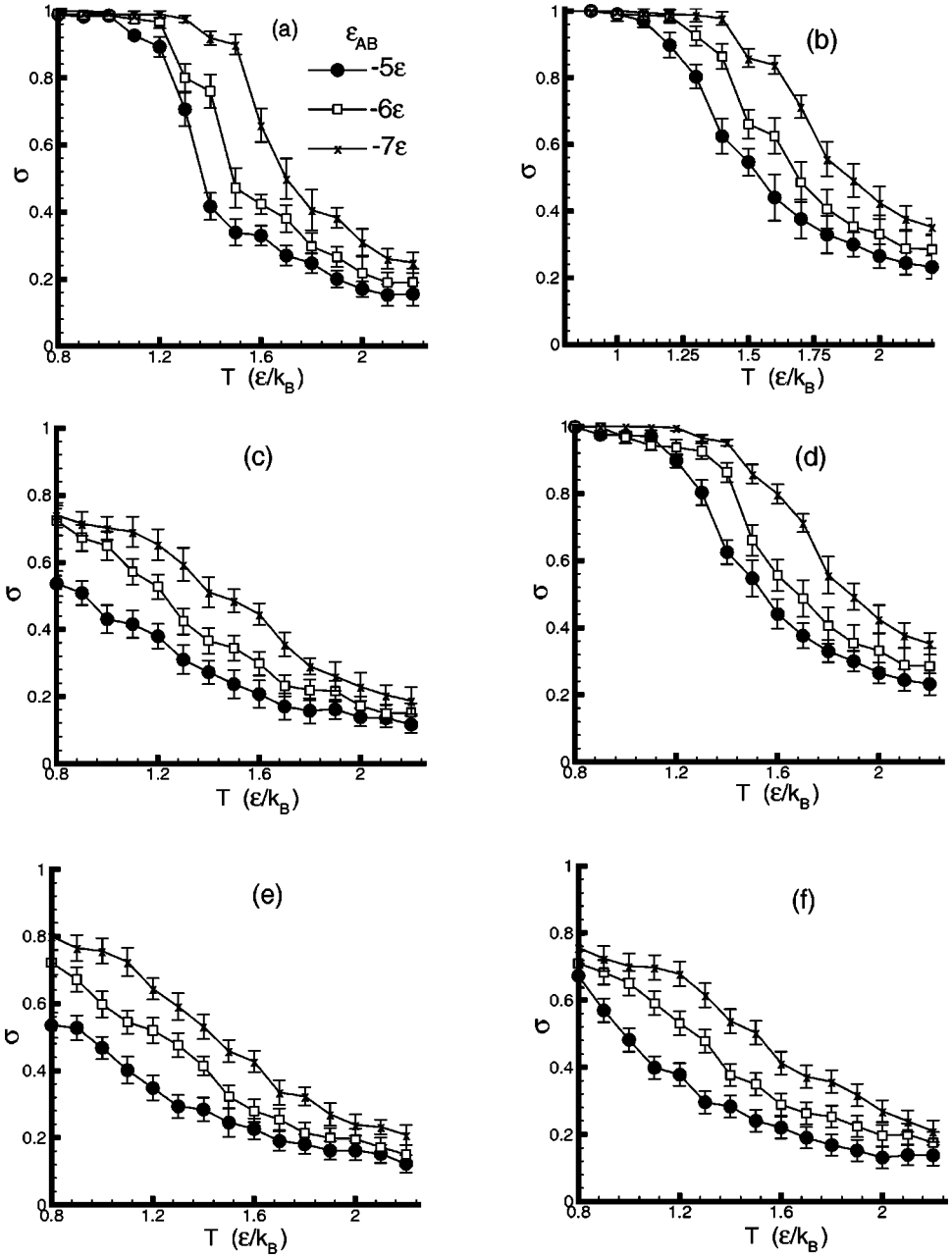

FIG. 10. Cowley short range order parameter, σ as a function of the inverse of temperature for different values of ε_{AB} with the reactor pressure of 10^{-6} ε/V for the same reactor conditions as in Fig. 3. The simulations were performed on (a) a {011} oriented, homoepitaxial substrate, (b) a {001} oriented, homoepitaxial substrates, (c) a {011} oriented, elemental substrate, (d) a {001} oriented, elemental substrate, (e) a {011} oriented, disordered substrate, and (f) a {001} oriented, disordered substrate. Error bars represent standard deviation over eight simulations at each temperature.

SHORT-RANGE ORDER

The short-range order evolves during growth. A convenient measure of the short-range order parameter for the CsCl lattice is that due to Cowley[22,23]

$$\sigma = -\frac{P_{AA} - n_A}{1 - n_A}, \tag{12}$$

where P_{AA} is the fraction of the nearest neighbor sites of an A atom that are occupied by A atoms (averaged over all A atoms), and n_A is the atomic fraction of A atoms in the entire film. With this definition, $\sigma = 1$ for the perfectly ordered CsCl lattice, $\sigma = -1$ for the phase separated system, and $\sigma = 0$ for a random solid solution of equal numbers of A and B atoms. If the number of A and B atoms are unequal, the magnitude of the extreme values of α are reduced. For the parameters used in these simulations, the perfect crystal order-disorder transition temperature is $T_c = \mu\varepsilon^*/k_B$ (within a second moment approximation,[24] where $\varepsilon^* = (\varepsilon_{AA} + \varepsilon_{BB})/2 - \varepsilon_{AB}$ and μ is a numerical constant that depends on lattice type ($\mu = 3.41$ for the lattice used here). For $\varepsilon_{AB} = -5\varepsilon$, -6ε, and -7ε, $T_c = 13.7\varepsilon/k_B$, $17.1\varepsilon/k_B$, and $20.5\varepsilon/k_B$, respectively.

Figure 10 shows the short range order parameter versus the growth temperature for six different substrates and three values of the bonding parameter ε_{AB}. This figure shows that the crystal is disordered at much lower (roughly one order of magnitude) temperature than expected based upon bulk thermodynamics. This is, in part, due to our approximation that the bulk is a frozen history of the growth surface. Nonetheless, this large difference is a clear indication that kinetic and equilibrium ordering are much different. One reason for this

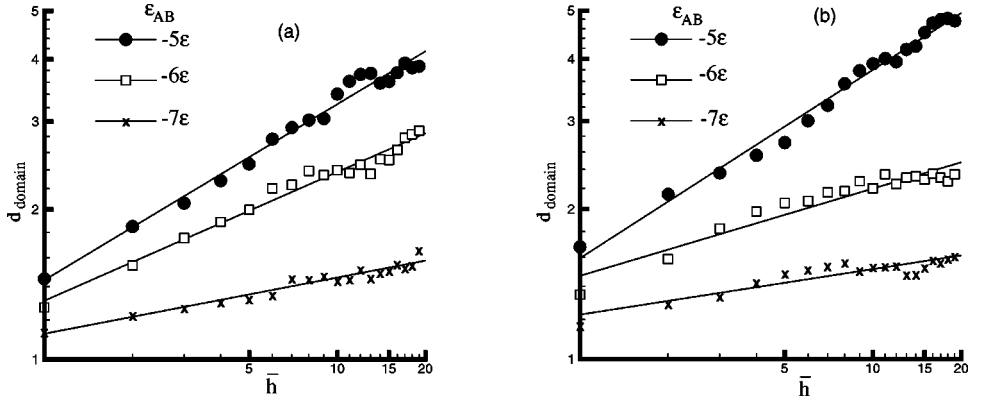

FIG. 11. Evolution of average domain size of films grown on elemental and disordered substrates for different values of ε_{AB} at a temperature of $1\varepsilon/k_B$, with the reactor pressure of 10^{-6} ε/V for the same reactor conditions as in Fig. 3. The simulations were performed on (a) a {011} oriented, elemental substrate and (b) a {011} oriented, disordered substrate. Both axes are plotted to logarithmic scale.

difference is that atoms on the surface have fewer bonds than do those within the bulk. However, this effect alone could not explain more than a factor of two change in T_c. The difference between the kinetic T_c and its equilibrium value is attributable to the magnitude of the barriers for the chemical reactions. If the barrier for diffusion is low (not examined here), we expect that the kinetic T_c will be significantly closer to the equilibrium surface T_c.

The growth on homoepitaxial substrates [Figs. 10(a) and 10(b)] produced perfectly ordered homoepitaxial films at low temperatures ($T \ll T_c$). As the temperature is increased, the films become increasingly disordered (all films in Fig. 10 are grown to a thickness of 32 atomic planes). This may be attributed to the fact that the difference between the deposition rates at ''right'' and ''wrong'' sites decreases with increasing temperature [see Eqs. (1) and (3)]. Similarly, the rate of etching is less site-selective at higher temperatures [see Eqs. (2) and (4)]. The order-disorder transformation occurs at higher temperatures with increasing $|\varepsilon_{AB}|$. This is not surprising since larger values of $-\varepsilon_{AB}$ imply larger driving forces for ordering.

The degree of short-range order in the films grown on elemental {011} [Fig. 10(c)] and disordered {011} and {001} surfaces [Figs. 10(e) and 10(f)] at low temperatures is considerably lower than for films grown on homoepitaxial substrates. This is because the short-range order in the vicinity of antiphase boundaries is considerably lower than in perfect crystals. A large number of islands (of random orientation) are nucleated on films grown on elemental and disordered substrates at small thicknesses, leading to a high APB density. {001} films grown on an elemental substrate [Fig. 10(d)] are nearly perfectly ordered at low temperature, since this film exhibits no antiphase boundaries (the flat growth surface is elemental).

DOMAIN SIZE

The linear domain size is plotted as a function of film thickness for (011) films grown on elemental and disordered substrates with several values of the *A*-*B* binding energy ε_{AB} (see Fig. 11). These simulations were performed under the same conditions as those used to produce Figs. 3–5, above. The domain size is calculated using the linear intercept method: a $[01\bar{1}]$ oriented line is drawn at the desired film height and the number of times an antiphase domain wall is crossed is counted Q. This number is averaged over 64 parallel lines and the average domain size d_{domain} is given by the dimension of the sample in the $[01\bar{1}]$ direction divided by $\bar{N}$.

The domain size in Fig. 11 increases in a nonlinear manner with film thickness. This dependence is well fit by a power law of the form

$$d_{\text{domain}} = a\bar{h}^n, \tag{13}$$

where a and n are determined by fitting to the data. The resultant fitting parameters are shown in Table II. n is found to be in the range of 0.09–0.38. Both a and n decrease with increasing $|\varepsilon_{AB}|$.

On {011} oriented film substrates, growth occurs by means of a step growth mechanism. Depositing atoms find more unlike neighbors at the outer surface of a curved APB than at the inner surface. Thus the rate of etching is slower at the outer surface of the APB. Therefore, domains boundaries should move toward their center of curvature. This curvature driven APB evolution leads to domain coarsening during film growth. If the APB migration rate was proportional to its curvature, we should expect $n = 1/2$. Since $n < 1/2$ in all cases, the boundary velocity must be a sub-linear function of the boundary curvature. The fact that n changes with ε_{AB} suggests that the dependence of the boundary velocity on curvature depends on several competing kinetic factors (e.g., island nucleation and step migration).

The number of domains formed at small film thicknesses is a function of the *A*-*B* binding energy ε_{AB} (see the values of the fitting parameter a in Table II). A stronger *A*-*B* bond leads to more stable *A*-*B* pairs on the substrate, independent

TABLE II. Fitting parameters for the power-law dependence of the domain size on film thickness on elemental and disordered substrates with {011} orientation $d_{\text{domain}} = a\bar{h}^n$.

Substrate	ε_{AB}	a	n
Elemental	-5ε	1.45	0.35
	-6ε	1.31	0.26
	-7ε	1.12	0.13
Disordered	-5ε	1.6	0.38
	-6ε	1.47	0.18
	-7ε	1.22	0.09

of the phase implied (i.e., A on the α or β sublattice). Increasing the ε_{AB} magnitude increases the stability of the small islands that nucleate on the substrate. Thus the initial domain size on the substrate surface increases with increasing ε_{AB}. As the strength of *A-B* bonds increases, atoms at the ''wrong'' sites are stabilized by the presence of a few unlike atoms. Thus the atoms depositing at the inner surface of an APB have a low etching rate even with some like neighbors. Thus the domain coarsening effect decreases with increasing $|\varepsilon_{AB}|$.

CONCLUSIONS

Optimization of the production of high quality epitaxial films by OMVPE techniques, requires both high film growth rates and low defect densities. The growth rate can be increased by either increasing the growth temperature or the gas pressure. Of these two, increasing temperature has a much larger effect since it enters the reaction rates within an exponential while the pressure only in the prefactor. Unfortunately, increasing the temperature increases the defect concentration, as measured by a decrease in the short-range order parameter. However, the average domain size (i.e., inverse antiphase boundary density) increases with increasing temperature because the island nucleation rate decreases with temperature and the rate at which the resultant antiphase boundaries coarsen increases with temperature. Overall, optimal growth is a compromise between high growth rates and high quality. Changing the substrate also modifies the film growth. Homoepitaxially grown films are typically better ordered than those grown on elemental or disordered substrates. This is largely due to the formation of antiphase domain structures on the nonhomoepitaxial substrates. Growth on {011} and {001} occur at nearly the same rates and produce films of similar roughness and short-range order. The only exception is that {001} films grown on elemental substrates and those grown homoepitaxially are indistinguishable, while this is not the case for {011} growth. This is because the {001} surfaces of the elemental and homoepitaxial substrates are identical (at the nearest neighbor level). The present simulations are highly idealized in many respects. They do not consider the effects of elastic misfit on heteroepitaxial growth, they do not incorporate diffusion, the reaction kinetics are assumed, no surface reconstruction is allowed, etc. Of these, the most intrinsic difficulty is obtaining realistic reaction kinetic information. First principles calculations could provide some of this type of information, although such applications are difficult for most OMVPE precursors.

[1] W. G. Breiland, M. E. Coltrin, J. R. Creighton, H. Q. Hou, H. K. Moffat, and J. Y. Tsao, Mater. Sci. Eng., R. **24**, 241 (1999).

[2] A. F. Voter, Phys. Rev. Lett. **78**, 3908 (1997).

[3] C. C. Battaile, D. J. Srolovitz, and J. E. Butler, J. Appl. Phys. **82**, 6293 (1998).

[4] C. C. Battaile, D. J. Srolovitz, and J. E. Butler, J. Cryst. Growth **194**, 353 (1998).

[5] C. C. Battaile, D. J. Srolovitz, and J. E. Butler, J. Mater. Res. **14**, 3439 (1999).

[6] M. E. Taylor and H. A. Atwater, Appl. Surf. Sci. **127–129**, 159 (1998).

[7] D. S. Cao, A. W. Kimball, G. S. Chen, K. L. Fry, and D. B. Stringfellow, J. Appl. Phys. **66**, 5384 (1989).

[8] W. J. DeSisto, E. J. Cukauskas, B. J. Rappoli, J. C. Colberton, and J. H. Classen, Chem. Vap. Deposition **5**, 233 (1999).

[9] W. A. Feil, B. W. Wessels, L. M. Tonge, and T. J. Marks, J. Appl. Phys. **67**, 3858 (1990).

[10] J. L. Blue, J. Vac. Sci. Tech. **16**(3), 1342 (1998).

[11] S. T. Coyle, M. R. Scheinfein, and J. L. Blue, Appl. Phys. Lett. **72**, 912 (1998).

[12] M. A. Gallivan, D. G. Goodwin, and R. M. Murray, Mater. Res. Soc. Symp. Proc (to be published).

[13] Y. Shim, D. P. Landau, and S. Pal, J. Phys.: Condens. Matter **11**, 10 007 (1999).

[14] G. H. Gilmer and P. Bennema, J. Appl. Phys. **43**, 1347 (1972).

[15] K. A. Fichtorn and W. A. Weinberg, J. Chem. Phys. **95**, 1090 (1991).

[16] A. B. Bortz, M. H. Kalos, and J. L. L. Lebowitz, J. Comput. Phys. **17**, 11 (1975).

[17] G. N. Hassold and E. A. Holm, Comput. Phys. **7**, 97 (1993).

[18] N. Metropolis, A. W. Rosenbluth, M. N. Rosenbluth, and A. H. Teller, J. Chem. Phys. **21**, 1087 (1953).

[19] A. Gomyo, T. Suzuki, and S. Iijima, Phys. Rev. Lett. **60**, 2645 (1988).

[20] P. Bellon, J. P. Chevalier, E. Augarde, J. P. Andre, and G. P. Martin, J. Appl. Phys. **66**, 2388 (1989).

[21] D. A. Porter and K. E. Easterling, *Phase Transformations in Metals and Alloys* (Chapman & Hall, New York, 1992).

[22] J. M. Cowley, J. Appl. Phys. **21**, 24 (1950).

[23] P. W. Rooney and F. Hellman, Phys. Rev. B **48**, 3079 (1993).

[24] L. A. Girifalco, *Statistical Physics of Materials* (Wiley Interscience, New York, 1973).